NUCLEAR INSTRUMENTS AND METHODS 145 (1977) 537-553 ; © NORTH-HOLLAND PUBLISHING CO.

ADDED PRECISION IN ^{57}Fe MÖSSBAUER SPECTROSCOPY

W. R. DUNHAM, C. T. WU, R. M. POLICHAR*, R. H. SANDS

Biophysics Research Division, Institute of Science and Technology, University of Michigan, Ann Arbor, MI 48109, U.S.A.

and

L. J. HARDING

University of Michigan Computer Center, Ann Arbor, MI 48109, U.S.A.

Received 23 March 1977

This paper contains (1) the necessary mathematics for a precise interpretation of Mössbauer data, and (2) a characterization of a spectrometer designed specifically to maximize the information available from these data. The innovative aspects of this spectrometer are that it provides a known absorber lineshape, that it is quantitative, and that it provides information on the vibrational states of the absorber via the second order Doppler shift vs temperature and the total absorption vs temperature. The spectrometer allows sample temperature and applied magnetic field to be varied in any combination of 2–350 K or 0–6 T, respectively. Simultaneous collection of four data streams allows an accurate representation of the transmission spectrum. Sophisticated computer treatment with extensive use of least squares fitting procedures and fast Fourier transform techniques provides the final output display of sample cross-section vs standardized source velocity. The cross-section display is shown to be independent of the thickness of samples with Mössbauer optical densities up to 3. In addition, we report the method and results of measurements which must precede the operation of the spectrometer: (1) the absorption coefficient of iron at 14 keV: $(498 \pm 7)\,\mathrm{cm}^{-1}$, (2) the Debye temperature of our source (^{57}Co in rhodium matrix): (361 ± 20) K, (3) the source lineshape: three Lorentzians with Heisenberg linewidth, a center line with twice the intensity of the symmetrically placed outer lines which are spaced 0.055 mm/s apart, (4) the Mössbauer effect cross-section for ^{57}Fe: $(2.4 \pm 0.2) \times 10^{-18}\,\mathrm{cm}^2$, (5) the Debye temperature of iron (NBS #1541): (430 ± 30) K, and (6) the values for the Hamiltonian parameters of iron metal (NBS #1541) at 290, 101 and 4.2 K. The precision of the determined Hamiltonian parameters is defined in terms of a statistic with a weighted χ^2 distribution.

1. Introduction

We have constructed an ^{57}Fe Mössbauer spectrometer whose final output is Mössbauer effect cross section vs standardized source–sample relative velocity. In order to achieve this result the spectrometer collects simultaneously four streams of data which are computer treated with extensive use of least squares fitting procedures and fast Fourier transform techniques. Furthermore, the machine has two other important properties: (1) it permits the measurement of the source lineshape and Debye–Waller factor, and (2) it allows the sample temperature and applied magnetic field to be varied in any combination of temperatures, 2–350 K, or fields, 0–6 T, independent of the source temperature or field. The chief result of this effort is Mössbauer data with more information content, with greater resolution, and presented in a form which is potentially directly comparable to other data.

The need for the machine arose from our previous research on a group of electron-transport proteins containing two iron atoms per molecule[1]). For example, we found that we could not precisely fit the spectra of these samples when the Mössbauer Hamiltonian consisted simply of a quadrupole interaction in an applied magnetic field. When we failed to fit these spectra by assuming a more complicated Hamiltonian, we began to suspect some inaccuracy in the data. In addition, we began work on proteins with four and eight iron atoms per molecule; thus our need for more accurate and precise data. We also felt that improvements in the quality of biological samples and in our ability to handle theoretically the complex Hamiltonians from these samples were outstripping the capabilities of the spectrometers; thus the need to improve the quality of our data and the machines which produced them.

The basic problem of the Mössbauer spectroscopist is to fit his data to his simulation program output. He may choose to do the fitting with a computer, but, for us, the complexity of the required Hamiltonians has often prohibited this method. Therefore, we fit by trial and error the

* Present address: Science Applications Inc., La Jolla, CA 92038, U.S.A.

plotted output of our simulation programs to the x–y data from the spectrometer. Our efforts have been directed toward making the x (velocity) and y (absorbance or cross-section) coordinates as accurate as possible.

In the following we shall describe separately the two axes with the component parts and mathematics necessary for their characterization. For the x-axis these consist of:

1) velocity drive,
2) Moiré fringe interferometer,
3) "zero-position" control circuit,
4) "zero-position" monitor circuit,
5) time channel,
6) "cosine broadening" correction,
7) 2nd-order relativistic Doppler shift correction.

For the y-axis these consist of:

1) signal channel [i.e., gas proportional counter, counting electronics, and corrections for pile-up, deadtime and background. A detailed description is not within the scope of this paper, but is presented separately[2])],
2) solid angle correction,
3) removal of source lineshape effect,
4) removal of the blackness effect,
5) Debye–Waller factor determination,
6) source lineshape determination.

Finally, we shall present some of the output of the machine which pertains to source and absorber standardization.

2. Overall characteristics

The general features of the dewar portion of this spectrometer are shown in fig. 1. The dewar plus superconducting solenoid and associated electronics was purchased from American Magnetics, Inc.[3]), who also built the solenoid and accessories. The dewar (Model CT-70) was manufactured by Cryogenic Associates[4]) with the exception of the solenoid bobbin which serves also as the lower and inner walls of the liquid helium chamber. The

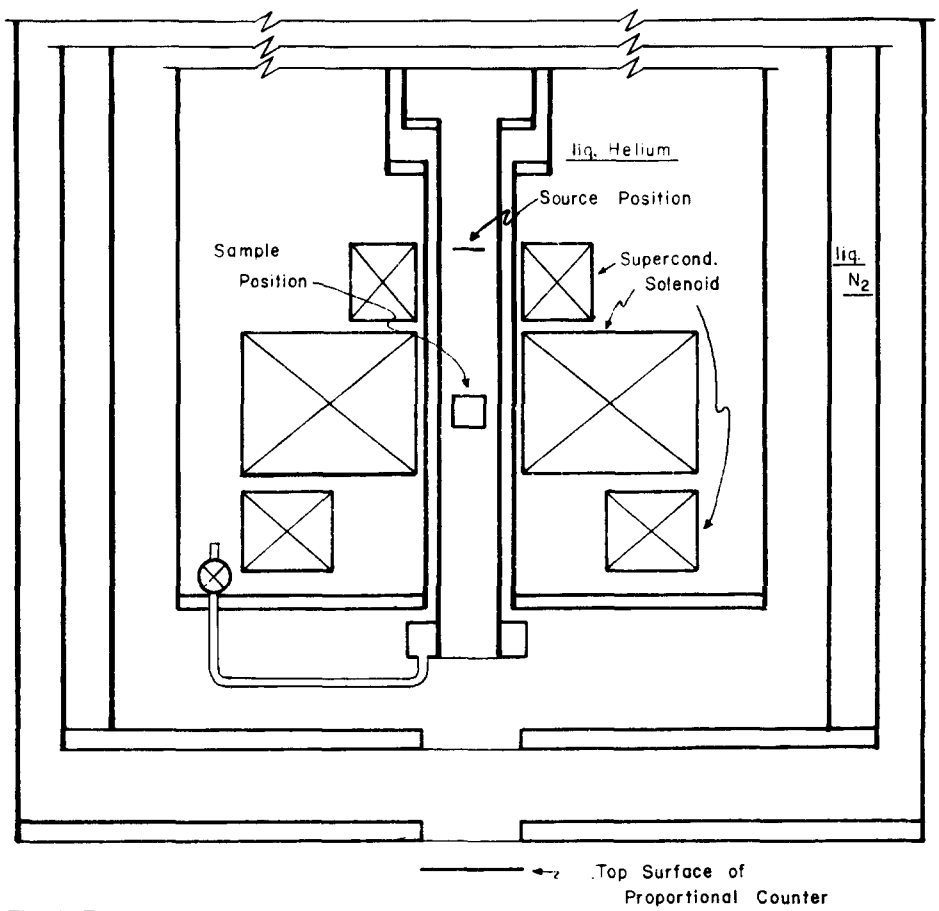

Fig. 1. Dewar geometry.

solenoid is a triplex configuration which provides simultaneously: a field maximum of up to 6.5 T at the sample position, a short field null (less than 0.1 T) at the source position, and a long field null (less than 0.1 T) over the counter volume. The solenoid also has the following accessories: (1) the triplex coil has a removable set of vapor-cooled current leads and a persistent mode switch at the top of the solenoid; (2) in the solenoid, there is another winding, also with removable leads, which provides fields up to 500 G to null any remnant field present when the triplex coil is not in use; (3) inside the solenoid, there is a winding which measures the field intensity from the triplex coil. Coarse temperature variation is accomplished by varying the amount of liquid helium into the sample chamber via a throttling valve at the bottom of the liquid helium chamber. In turn, the throttling valve is manually controlled at the top of the dewar. Sample temperature control is effected electronically by a heater and sensor arrangement in the sample holder. Sample access is through the top of the sample chamber. The drive mechanism (fig. 2), which is outside the dewar, can be lifted and with it the drive extension and the entire sample holder are also removed.

We have used machineable tungsten for the collimators to provide an additional safety margin when the drive is outside the dewar and to eliminate radiation reaching the counter by any other route than through the sample. The gamma-ray beam is collimated at the bottom of the sample such that the beam does not impinge on any metal surface of the counter or the dewar. The machineable tungsten "can" around the source has two additional functions. Due to the proximity of the source and sample, the tungsten "can" around the source provides needed thermal resis-

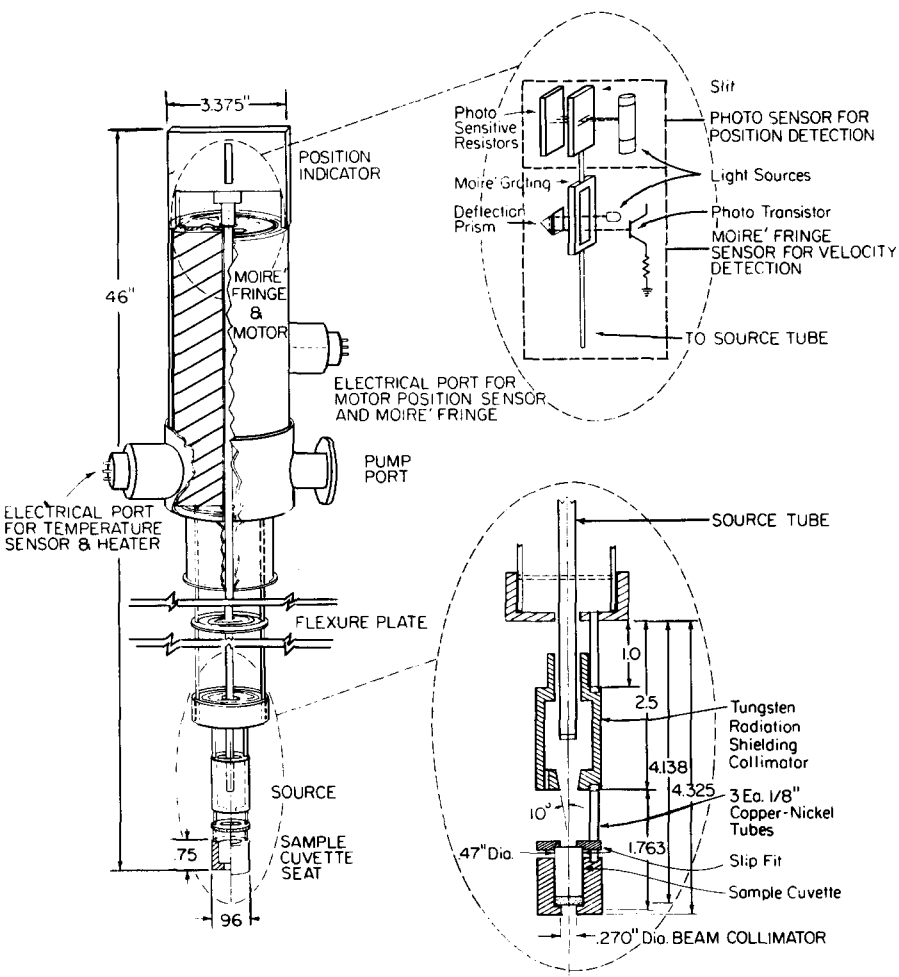

Fig. 2. Drive assembly.

TABLE 1
System specifications.

Upper bound of scan range	200 mm/s
Lower bound of scan range	1.5 mm/s
lN use rate	0.3 l/h
lN capacity	7 l
lHe use rate	0.3 l/h
lHe capacity	10 l
Maximum solenoid field intensity	6.5 T
Current at maximum field	62.5 A
Moire fringe grating frequency	2000 lines/in.
Temperature stability at sample and source	0.1 K
Dwell time per channel	5 ms
Count rate with 35 mCi source	20 kHz
Time to collect 100 000 counts per channel for normal biological sample	21 min
Optimum amount of sample	2 μmol ^{57}Fe

tance to isolate the two heaters. Inside the "can", there is a polyethylene bucket which excludes liquid hellium from the source when the sample chamber contains liquid helium. The presence of liquid helium at the source has two detrimental effects: (1) since the source moves during a velocity sweep, it creates a non-trivial change in the non-resonant scattering cross section as a function of source position, and (2) since it is necessary to hold the source temperature above 5 K to avoid magnetic splitting in the source, the presence of the liquid near the source would result in constant boiling at its surface. A carbon resistor–thermistor pair is mounted immediately behind the source to monitor the temperature of the source. We show the overall system performance specifications in table 1.

3. The "x-axis"

The main part of the drive (enclosed in dashed lines in fig. 3) is a Ranger Instruments[5]) velocity drive (Model MS/VT-700) operated in the constant acceleration, flyback mode.

We synchronize the analyzer [Model NS900/NS458, Northern Scientific[6]] to the drive by converting the binary address to a very precise voltage; this voltage, in turn, becomes the reference ramp in the velocity drive servo system (see fig. 3). We note in passing that although the multichannel analyzer provides an analog representation of the horizontal axis, we were forced to use the seven most significant bits in a 12-bit digi-

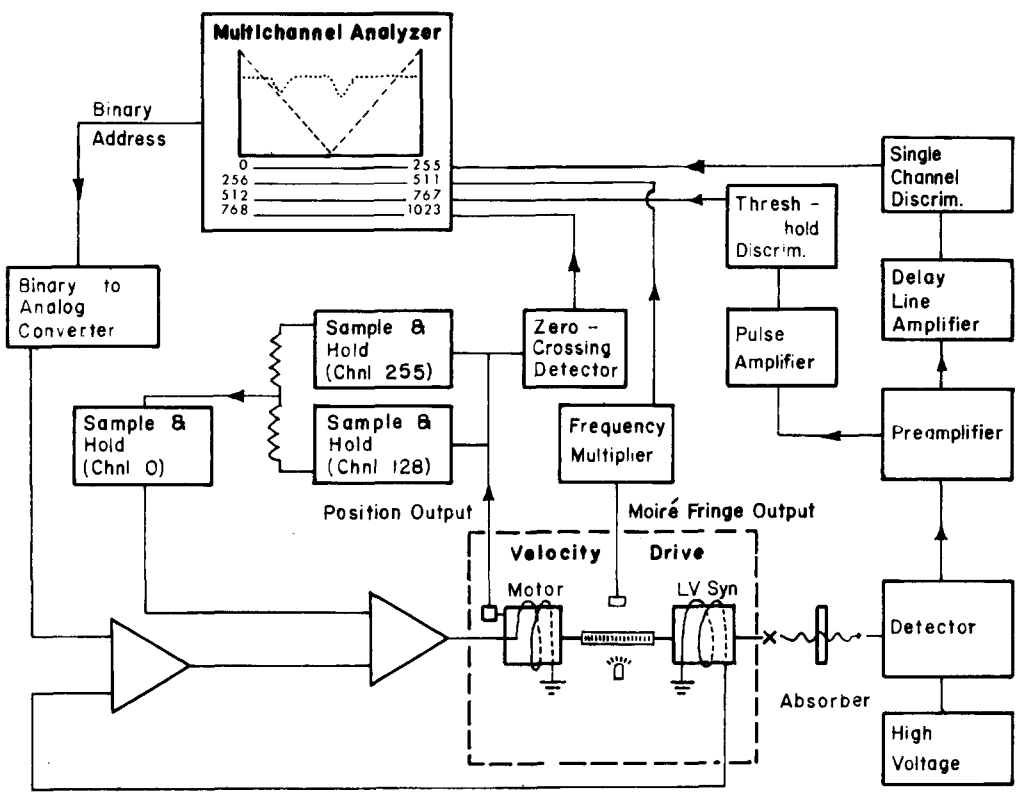

Fig. 3. Block diagram of electronics.

tal/analog converter in order to bring the precision of this ramp to a level which is comparable to the precisions of the other parts of the spectrometer.

In order to measure the relative position changes of source to absorber during a velocity sweep, the Ranger drive incorporates a Moiré fringe interferometer into the housing of the drive motor. The Ranger drive electronically derives a pulse output from the interferometer whose frequency is eight times the rate at which fringes pass a stationary point. This pulse output is stored in the second subgroup of the analyzer.

In order to maintain a known relative position between source and collimator, we have mounted a position transducer at the top of the drive. We derive the average of the extremes of the position output and sum it into the source drive servo loop with a sample and hold circuit. In this way we add a correction to the sweep which is constant during any one sweep. In addition, we also generate a pulse whenever the position transducer output crosses "zero". The pulse is collected in the fourth subgroup of the analyzer in order to provide a record of the drive stability and to identify the channels which correspond to zero position. From these channel numbers and the velocity output one can calculate the absolute source collimator distance corresponding to each channel.

Since the information which describes the position of the drive at any channel is contained in the second and fourth subgroups of the analyzer, we need only measure the time duration of any channel in order to determine the velocity at any channel. A pulse output from a crystal controlled oscillator is multiplexed into channel 258 of the analyzer. We show the performance specifications of the velocity drive in table 1. The details of the electronics can be found in the thesis[7]) of Chu Tzu Wu.

The raw data which characterizes the motion of the source must be corrected in two ways before one can properly define the "x" or velocity axis of the spectrometer. The corrections applied by the computer program are described in the following paragraphs. The first correction is for the effect of cosine broadening. Cosine broadening is the descriptive term for the difference between source-absorber velocity and average Doppler velocity when the source and absorber are not assumed to be points. The Doppler velocity is equal to the component of the source velocity, v, along the direction of the gamma ray. Therefore, the average value of the Doppler velocity is equal to $v\langle\cos\theta\rangle$, when θ is the angle of the source motion to the gamma-ray. When the source is finite, a closed form calculation of $\langle\cos\theta\rangle$ is impossible. However, a good approximation can be derived by integrating the power series expansion of cos θ. Hence,

$$\langle\cos\theta\rangle = 1 - \frac{a^2+b^2}{4d^2} = 1-\eta, \tag{1}$$

where a is the source radius, b is the collimator radius and d is the source-to-collimator distance. Although d changes during a sweep of the spectrometer, these changes are so small that $\langle\cos\theta\rangle$ can be assumed to be constant: for our machine, η equals 7.7×10^{-4}.

The final correction made to the velocity data is that from the second order relativistic Doppler shift. By correcting the energy of the emitted gamma ray for time dilation of its frame relative to the stationary absorber frame, we can write the following expression for the energy of the emitted gamma in the absorber frame:

$$E = E_\gamma\left(1+\frac{v}{c}\right)\left(1-\frac{\langle v^2\rangle}{2c^2}\right), \tag{2}$$

where E_γ is the energy of the nuclear transition; v is the source velocity (caused by the source mover), $\langle v^2\rangle$ results from the "thermal" velocity of the emitting nucleus. The correction from thermal effects is called the second-order relativistic Doppler shift, although it is not the second order shift due to the drive velocity (the second-order shift from the drive velocity is negligible). A similar correction must be made for the thermal motion of the absorbing nucleus.

Since the major contribution to $\langle v^2\rangle$ in this term is nuclear vibrational motion, we can derive an approximate expression for $\langle v^2\rangle$ from the Debye model for solids. The expression used by us for the temperature dependence of the velocity shift from second-order Doppler shift is:

$$\Delta v(T) = \frac{-\langle v^2\rangle}{2c} = \frac{-3kT}{2mc} D\left(\frac{\theta_D}{T}\right), \tag{3}$$

where the Debye function[15]) is adequately described by

$$D(R) = \frac{3}{R^3}\sum_{n=1}^{30}\frac{1}{n^4}\left[6-\exp(-nR)\left\{(nR)^3+3(nR)^2+\right.\right.$$
$$\left.\left.+6nR+6\right\}\right]. \tag{4}$$

The validity of the above expression is dependent on two assumptions: (1) that the Debye mod-

el for solids is appropriate to the sample and (2) that the expression for internal energy from the Debye model is a valid representation for this measurement which is performed at constant pressure rather than at constant volume. Since our equation for the "thermal" Doppler shift implies these restraints, we use it primarily as a definition for the parameter, θ_D, rather than as a theoretical derivation of the shift from the Debye model.

The temperature dependence in this expression necessitates the definition of a standard isomer shift. While we recognize that our definition is somewhat arbitrary, we feel it is a good compromise between (1) a method for separating the parameters belonging to the sample from those which are a property of the measuring system, and (2) a lack in the theory describing the phonon spectra of solids. In other words, we are able to separate the second-order Doppler shift from our own isomer shift values. Therefore we can be much more sensitive to temperature dependencies in the isomer shift which reflect real changes in bonding than we could previously. In addition, we can report the value of θ_D as a measured parameter. However, the cost of this procedure is that we have begun a system which requires that we measure the θ_D for our source and each of the absorbers.

Our standard reference material is iron-foil (NBS#1541) at 298 K. The isomer shift of this material is defined as the velocity zero of the spectrometer. The following equations show the way that our standardization is accomplished.

$$\delta(T, T') = \delta_{abs}(T) + \Delta v_{abs}(T) - \delta_{sou}(T') - \Delta v_{sou}(T'). \tag{5}$$

A relative isomer shift, $\delta(T, T')$, can be defined in this way for an absorber at temperature, T, and a source at temperature, T'. In order to specify a standard isomer shift we measure the isomer shift of Fe (NBS#1541), δ_{Fe}, with both the source and iron foil at 298 K. Finally, we define the standard isomer shift, δ_{stand}, as the directly measured isomer shift, $\delta(T, T')$ with absorber temperature, T, and sample temperature, T', corrected for the isomer shift of NBS#1541 and corrected to a source and sample temperature of 298 K.

$$\delta_{stand} = \delta(T, T') - \delta_{Fe} + \Delta v_{abs}(298) - \Delta v_{abs}(T) - \Delta v_{sou}(298) + \Delta v_{sou}(T'). \tag{6}$$

Thus this "standard" isomer shift will be identical to that made with both sample and source at room temperature quoted relative to iron foil.

4. The "y-axis"

The design considerations encountered in the construction of the gas counter and associated electronics for the signal channel are described in a separate paper[2]). It is sufficient to mention that the counter was a locally constructed, argon filled, end-on illumination, proportional gas counter and that all the electronics following the counter are manufactured by Ortec[8]). Tail pulses formed by the charge sensitive preamp at the counter follow two different pathways to the analyzer: (1) the "slow channel" has a 1 μs delay-line shaping amplifier and a timing single channel analyzer, (2) the "fast channel" has a 200 ns shaping amplifier and a threshold discriminator set to a voltage corresponding to a gamma-ray energy around 2 keV. Pulses from the discriminators of the slow and fast channels are collected in the first and third subgroups of the analyzer respectively (fig. 1).

The slow channel data is corrected for pileup errors by the fast channel data via the following expression:

$$I = \frac{I_{slow}}{1 - \tau \cdot I_{fast}}, \tag{7}$$

where I, I_{slow} and I_{Fast} are the corrected, slow and fast count rates, respectively, and τ is an effective counting loss time for the slow channel (1.1 μs). Justification for this correction is provided in the paper[2]) which deals with the signal channel. Note that both the fast and slow channels contain the Mössbauer spectrum. Therefore. the pileup correction is not constant and will depend on the particular shape of the Mössbauer spectrum. Failure to make a "dynamic" pileup correction of this kind can result in a severe distortion of the Mossbauer spectrum, especially in instruments with high incident count rates at the detector.

The gamma-ray beam collimator which defines the beam at the counter is located at the sample (see fig. 3). The motion of the source relative to the sample creates a dependence of the beam solid angle on the channel number. Corrections for changing solid angle take many forms among Mössbauer laboratories; however, the solid angle correction performed by us has some positive qualities worth mentioning. By collimating at the sample, we minimize the possibility that an inhomogeneity in the sample can cause a depen-

dence of the cross-section on solid angle. In addition, the "zero position" regulator maintains a well-defined distance between the source and collimator so that by using the information in subgroups two and four in the analyzer, we can make the solid angle correction with the following expression:

$$\frac{\Omega}{4\pi} = \frac{1}{4}\left(\frac{\varepsilon^2}{1+\frac{1}{2}\varepsilon^2}\right), \tag{8}$$

where $\Omega/4\pi$ is the fractional solid angle, ε is the ratio of the collimator radius to the source–collimator distance.

By checking on whether this expression actually removes the solid angle effect, we have a means of verifying that the beam is not being collimated elsewhere in the system. For example, if the counter's physical dimensions are such that the solid angle effect modifies the effective length of the counter, a very complex problem is created in trying to remove the dependence of counter absorption on solid angle. This type of problem occurs only when the efficiency of the counting gas is marginal, so that a sizeable fraction of the radiation can escape through the counter side walls as in our situation using argon as a counting gas.

The previous sections on the "y-axis" have dealt with the problem of correctly representing the counting data as those from a transmission spectrometer. In the following sections, we deal with the problem of converting this information to a measurement of sample absorption.

We define the interaction between the gamma-ray beam and sample as follows:

$$I(v) = I_0(1-f_s) + I_a + f_s I_0 \int_{-\infty}^{\infty} S(v-E) \times \times \exp[-\sigma(E)\, t_a]\, dE, \tag{9}$$

where $I(v)$, I_0 and I_a are the pileup and solid angle corrected count rate, the detected 14 keV gamma-ray count rate, and the non-14 keV gamma-ray count rate, respectively. f_s is the Debye–Waller factor for the source, and the integral is the transmission integral for Mössbauer spectroscopy, $T(v)$, with $S(E-v)$ being the source shape function, σ the differential Mössbauer cross section of the absorber, and t_a the absorber areal density (including the Debye–Waller function). I_a results almost entirely from Compton processes in the counter induced by 122 keV gamma-rays. (One of the main reasons for selecting argon as a counting gas is its property of minimizing the relative contribution of I_a.) To find the value of I_0 and I_a we take a value of $I(v)$ from the spectrum where $T(v)=1$, usually the left or right extreme of the spectrum, and then solve an equation for I_0 and I_a which models the emission spectrum of the source and the scattering cross-section of the absorber. The equation for the model is found by running "Mössbauer" spectra on Pb, Cu and Al to establish the intensities at 122, 136, 6.5, 20 and 14 keV. (20 keV is the rhodium X-ray line from the source.) We assume that our biological samples have the scattering cross-sections of water and make a correction for age of the source. Although this process was time-consuming to construct, the information obtained from it has allowed us to construct a system which can provide a background level as low as 3% of the total counts in the signal channel. A low value of I_a is especially important in the formation of the transmission array.

By solving eq. (9) for $T(v)$ we obtain the following expression:

$$T(v) = [I(v) - I_0(1-f_s) - I_a]/f_s I_0\,. \tag{10}$$

$T(v)$ is the transmission spectrum which is implied, but not actually represented, by most published spectra. That is, if one looks at a spectrum in the literature which shows a spectral minimum of 85% transmission, the tendency is to assume that the spectrum is undistorted by the blackness effect since $0.86 = \exp[-0.15]$. However, if f_S or I_a is large, the 85% transmission reported can be 40%, for example. The result is a spectral distortion which is further enhanced by the convolution of the source and absorber functions. More will be made of this effect later as we discuss the deconvolution of the source shape function from the transmission integral.

The transmission integral as defined in eq. (9) poses a difficult problem for the Mössbauer spectroscopist. The information desired from the experiment is $\sigma(E)$, the cross-section. The integral is the convolution of the source shape function $S(v-E)$, and the transmission function for the absorber, $\exp[-\sigma(E)t_a]$. Since t_a and $S(v-E)$ can be measured and since $\sigma(E)$ can be calculated by a computer program, several investigators have chosen to perform the convolution of the source shape with a guess at the parameters which give rise to $\sigma(E)$, fit the experimental data to the trial function and then use χ^2 or some like criterion to gauge the precision of the fit and choose the parameters for the next trial. This trial and error

procedure should, by minimizing χ^2, eventually result in a determination of the maximum amount of information on the parameters which give rise to $\sigma(E)$. This procedure, i.e., curve fitting the transmission integral, has several drawbacks with respect to its alternatives:

1) It assumes that the $\sigma(E)$ generating program contains the necessary sophistication to generate a "correct" $\sigma(E)$. If the sample is assumed to contain a single iron environment, then the total number of possible free parameters in $\sigma(E)$ is fifteen. However many experiments do not provide prior information (i.e., EPR and ENDOR measurements) on how many "free" parameters are free. Specifically, it is extremely difficult to determine whether a sample contains a distribution in one of these parameters "G-strain", for example.

2) Since $\sigma(E)$ is itself a convolution, calculation of the transmission integral requires an additional convolution for each trial in the curve fitting procedure. This extra convolution is an expensive complication to a curve fitting procedure.

3) The exponential in the transmission integral is an especially malicious property as it forces the curve fitter to determine the magnitude of the value being exponentiated either by experiment or by trial and error. Since this experiment is often impossible, another free parameter is added to the curve fitting procedure.

The most attractive alternative to the above procedure is deconvolution of the transmission integral by a Fourier transform. The advantages of deconvolution are that the curve fitter is placed one step closer to the Mössbauer Hamiltonian parameters and can test more easily the effects of subtle parameter variation in the sample. Deconvolution by a Fourier transform is, however, fraught with mathematical difficulties. In the following section, we show how these difficulties can be circumvented by stabilizing the Fourier transform with a truncation in Fourier space.

In the previous section, we have sketched briefly the method by which we use the information from the multichannel analyzer to construct an array, v, for the velocity at each channel and an array, T, for the transmission of the spectrometer at each channel. Together these two arrays constitute a discrete representation of the function $T(v)$ in eq. (10). In reality, the formation of $T(v)$ is computationally more complicated than is shown.

In order to demonstrate the method we first rewrite eq. (10) as:

$$1 - T(v) = \frac{[I_{av} - I(v)]}{f_s(I_{av} - I_a)}, \tag{11}$$

where $I_{av} = I_0 + I_a$. Remembering that I_{av} is derived from the left or right extremes of the data, $I(v)$, in order for an average of $I(v)$ to equal I_{av}, $T(v)$ must equal one. In real spectra this is not true unless the experimenter pays the price of greatly extending the scan range. Of course, the reason for this is the wings of the resonances in the spectrum. We can describe these resonances mathematically as:

$$1 - T(v) = \sum_{j=1}^{m} \frac{a_j}{b_j^2 + (x_j - v)^2}, \tag{12}$$

where b_j is the linewidth, x_j is the resonance center, and a_j is a height parameter for the jth resonance. In order to estimate the value of $T(v)$ at the range extreme where I_{av} is derived, we fit $I(v)$ with a least-squares routine at its minima. Since a Lorentzian lineshape is inconvenient for this fit, we perform the following modification to the $T(v)$ array to make it compatible with a quadratic least-squares fitting routine:

$$\frac{1}{1 - T(v)} \simeq \sum_{j=1}^{m} \left(\frac{1}{a_j}\right) v^2 + \left(\frac{-2x_j}{a_j}\right) v + \left(\frac{b_j^2 + x_j^2}{a_j}\right). \tag{13}$$

The equation is accurate only in regions where the lines do not overlap. The procedure is to fit the minima of the $T(v)$ array to the form of eq. (13) by least squares. Then by evaluating the functional form of $T(v)$ at the v where I_a was derived, we can calculate a new I_{av} which is more accurate than the statistical uncertainty at any channel. With this new value for I_{av} we can recalculate $T(v)$. However, a more accurate evaluation of $T(v)$ is not the only reason for pursuing the elaborate procedure shown above. Another reason for this treatment (the one most pertinent to the present discussion) is that it provides an accurate description of the strongest spectral line. This information is important in finding the proper truncation point in Fourier space as will be shown below.

The convolution theorem of Fourier transform theory states that the convolution of two functions is the inverse transform of the product of the Fourier transforms of the two functions. Hence, one can deconvolve a function by taking its Fourier transform dividing it by the transform of the deconvolving function and then taking the inverse transform of the quotient. In reality, this process is performed via the discrete Fourier trans-

form[9]), which is the discrete representation of the Fourier series for a function. In the following, we shall treat the discrete transform and the integral transform as interchangeable, in order to maintain the functional form of the transmission integral. [This approximation can be formally justified[9].] We shall then show how the conclusions of this treatment fared when tested by the discrete transform process.

Invoking the convolution theorem of Fourier transforms, we find that:

$$F[T(v)] = F[S(E)] \cdot F[\exp\{-t_a\,\sigma(E)\}], \tag{14}$$

where the shape function

$$S(E) = \frac{\Gamma_s}{\pi(\Gamma_s^2 + E^2)}, \tag{15}$$

and

$$F[S(E)] = \exp(-|\Gamma_s t|), \tag{16}$$

where t is the abscissa of the Fourier space. Here it is shown to be a Lorentzian (Cauchy distribution). The use of more complex functional forms for $S(E)$ does not affect the validity of the following treatment; in fact, the exact functional form used by us is not Lorentzian and will be described later because its introduction at this point needlessly complicates the mathematics. In principle, one could find $\sigma(E)$ from the following equation:

$$\sigma(E) = \frac{1}{t_a} \ln\left\{F^{-1}\left[\frac{F[T(v)]}{\exp(-|\Gamma_s t|)}\right]\right\}. \tag{17}$$

However, the addition of "noise" to the problem prevents things from being so simple. The principal noise source in Mössbauer spectroscopy is the indeterminacy in the lifetime of any particular decaying nucleus. The noise properties which are important to us here are that it is "white"; i.e., the variance of the noise, s^2, which is constant in both the frequency and time domains, and it equals the number of counts collected in the measurement at any channel. We define a random function, $\eta(E)$, which has a $\langle\eta(E)\rangle = 0$ and a $\langle\eta^2(E)\rangle = s^2$, which is independent of E.

We write the total absorption function of the absorber as

$$A = \exp\left(-t_a \Gamma_a^2 \sum_{j=1}^{m} \frac{S_j}{\Gamma_a^2 + (E - E_j)^2}\right), \tag{18}$$

where m lines contribute to the cross-section; Γ_a, the absorber linewidth, and E_j, the resonant energy of the jth line, are given in terms of the number of channels, and S_j are constants which describe the intensity of each line.

Then, since $T(v)$ and $\eta(v)$ are independent and since the Fourier transform is a linear transformation, the Fourier transform of the transmission integral plus noise is

$$F[T(v) + \eta(v)] = F[S(E)] \cdot \cdot F\left[\exp\left(-\sum_{j=1}^{m} \frac{S_j \Gamma_a^2}{\Gamma_a^2 + (E - E_j)^2}\right]\right] + F[\eta(v)]. \tag{19}$$

If E is given in units of a channel width, we can write the integral transform using the kernel of the discrete transform, and setting the limits of the integral transform equal to the limits of the discrete transform, the Fourier transform becomes

$$F = \frac{\Gamma_s}{\pi} \int_{-\frac{1}{2}N}^{\frac{1}{2}N} \frac{\exp(2\pi i E t/N)}{\Gamma_s^2 + E^2}\,dE \cdot \cdot \int_{-\frac{1}{2}N}^{\frac{1}{2}N} \exp\left(-\sum_{j=1}^{m} \frac{S_j \Gamma_a^2}{\Gamma_a^2 + (E - E_j)^2}\right) \times \exp(2\pi i E t/N)\,dE + + \int_{-\frac{1}{2}N}^{\frac{1}{2}N} \eta(E) \exp(2\pi i E t/N)\,dE, \tag{20}$$

where N is the number of channels in the transform. If Γ_a and Γ_s are much less than N and if the argument of the exponents in the absorption function is much less than one, then the fourier transform becomes

$$F = \exp(-|2\pi\Gamma_s t/N|)\,\{F(0) - \Gamma_a \pi \sum_{j=1} S \times \times \exp(-|2\pi\Gamma_a t/N|) \exp(2\pi i E_j t/N)\} + \eta'(t), \tag{21}$$

where $\eta'(t)$ is another random function with $\langle\eta'\rangle = 0$ and $\langle\eta'^2\rangle = Ns^2$.

Dividing by $\exp[-|2\pi\Gamma_s t/N|]$ then yields the functional form of the deconvolved signal plus noise in Fourier space

$$F' = F(0) - \pi\Gamma_a \exp(-|2\pi\Gamma_a t/N|) \times \times \left\{\sum_{j=1}^{m} S \exp(2\pi i E_j t/N)\right\} + + \eta'(t) \exp(|2\pi\Gamma_s t/N|). \tag{22}$$

From eq. (22) the problem with Fourier transform deconvolutions is obvious: as t moves from zero the noise grows exponentially while the signal diminishes exponentially. Thus there is some t where the noise is greater than the signal. We

have chosen to truncate the transform at this point. Although truncation introduces a distortion to the backtransformed Lorentzian in the absorber cross-section, this distortion is accurately calculable as will be shown below.

One alternative to truncation is multiplying the above transform by a Gaussian shape function[10]). This method, which is intrinsically a convolution, has the desirable effect of eliminating the transform at highest t. However, the resulting lineshape requires the curve fitter to perform an additional convolution, the avoidance of which is one of the reasons to use Fourier transforms in the first place. In addition, the effect of the exponentiation in the absorption function is greatly complicated by convolving the Lorentzians with a Gaussian.

There is tremendous leeway in the choice of method for deriving the truncation point. With any choice the basic idea is to truncate the Fourier space before the noise component is much larger than the signal component. We have chosen the truncation point to be where the standard deviation of the noise equals the absolute value of the signal. The standard deviation of the noise is derivable in closed form. Following the logic in the appendix, one can show that the standard deviation of the noise σ_N, is:

$$\sigma_N = sN^{1/2} \exp(|2\pi\Gamma_s t/N|). \tag{23}$$

Deriving the absolute value of the signal is much more ambiguous than the derivation for noise height. Inspection of eq. (22) shows that the elements of the Fourier transform array are complex. One can show that the absolute magnitude of the elements must fit the following fluctuation formula:

$$|\text{signal}| \doteq \pi\Gamma_a C \exp(-|2\pi\Gamma_a t/N|). \tag{24}$$

The values of C and Γ_a can be determined by least-squares fitting the portion of the Fourier space which is dominated by the signal. This least-squares fitting procedure is used by us at the end of our program to provide a measured value for Γ_a; however, our method for deriving the signal height in Fourier space involves the curve fitting procedure used previously to correct the value of I_{av} during the construction of the $T(v)$ array.

From the previous curve fitting procedure, we know the height and linewidth of each of the principal lines in the Mössbauer spectrum. The strength of any resonance is proportional to its area rather than height. Thus, the magnitude of the Fourier transform of the jth line can be written as

$$|\text{signal}| = \frac{\pi a_j}{b_j \Delta v} \exp(-|2\pi\Gamma_a t/N|), \tag{25}$$

where a_j and b_j are defined in eq. (12), and Δv is the velocity increment between channels. By setting eqs. (23) and (25) equal and then solving for t we arrive at the truncation point:

$$T = \frac{N}{2\pi(\Gamma_a+\Gamma_s)} \ln\left(\frac{\pi a_j}{b_j \Delta v s N^{1/2}}\right). \tag{26}$$

We choose j such that the ratio of a_j to b_j is largest; therefore, our choice is equivalent to choosing the truncation point as the point where the noise amplitude equals the signal amplitude for the strongest line in the Mössbauer spectrum. Having found the truncation point, it is now possible to calculate the backtransform of the signal and the noise. We write the backtransform of a single line as

$$\begin{aligned} F^{-1}(j\text{th line}) &= \frac{1}{N}\int_{-T}^{T} \pi\Gamma_a \exp(-|2\pi\Gamma_a t/N|)\, S_j \times \\ &\quad \times \exp(2\pi i \Delta x t/N)\, dt \\ &= \frac{S_j\Gamma_a^2}{\Gamma_a^2+\Delta x^2}\left\{1 - \exp(-\Gamma_a T^*) \times \right. \\ &\quad \left. \times \left[\cos(\Delta x T^*) - \frac{\Delta x}{\Gamma_a}\sin(\Delta x T^*)\right]\right\}, \end{aligned} \tag{27}$$

where $\Delta x = E_j - x$, $T^* = 2\pi T/N$.

This function although not a pure Lorentzian is easily calculable and easily incorporated into Mössbauer spectral synthesis programs as the shape function for the emission lines from a particular nuclear configuration. The derivation shown above is for small S; however, by testing the deconvolution procedure with computer generated test spectra, we have shown that the inaccuracy in the form of eq. (27) is negligible if S_j is less than three. Several points concerning the above can now be emphasized to advantage. If the process in eq. (17) is performed on real data with truncation, one obtains $\sigma(E)$ in discrete form. The least-squares analysis of eq. (24) on the Fourier transform of this output will determine Γ_a to a precision which is calculable from the least-squares procedure. Thus Γ_a can be determined, which eliminates one of the variables in the curve fitting procedure. Furthermore, a more sophisticated analysis in the Fourier space can yield informa-

tion on parameter "fluctuations" (section 1) since the moments of a distribution are obtainable in the Fourier space[11]). The success of such a treatment would depend critically on the amplitude of the noise; however, parameter fluctuation can be a problem of such magnitude that its possibility of analysis in Fourier space is well to keep in mind.

It is worth mentioning at this point that a knowledge of the form of eq. (24) is unnecessary for successful data reduction of Mössbauer data. The sequence in most Mössbauer spectral synthesis programs is the generation of a line spectrum followed by a convolution for the absorber lineshape. The most accurate and efficient method of performing the convolution is the Fast Fourier Transform algorithm. In this case, one can accurately match the true form of the lineshape in eq. (27) by convolving the line spectrum with a Lorentzian lineshape and truncating the Fourier space.

Another important property of the above process is its effect on noise. After division by the source function in Fourier space, the standard deviation of the noise is given by eq. (23) [see p. 167, Cramer[12])]. We now calculate the mean variance in the Fourier space as

$$\bar{V} = \frac{1}{T}\int_0^T Ns^2 \exp(4\pi\Gamma_s t/N)\,\mathrm{d}t$$

$$= \frac{N^2 s^2}{4\pi\Gamma_s t}[\exp(4\pi\Gamma_s T/N) - 1]. \qquad (28)$$

Backtransforming the variance will simply multiply it by the number of degrees of freedom in the Fourier space, $2T$. In order to maintain the unitary quality of the dscrete transform[9]), we also multiply by $1/N^2$. Thus the final form of the variance is

$$\bar{V}' = \frac{s^2}{2\pi\Gamma_s}[\exp(4\pi\Gamma_s T/N) - 1]. \qquad (29)$$

If $T = \frac{1}{2}N$, *then* $\sqrt{\bar{V}'}$ is always greater than s, the rms noise in the original spectrum. The amount of signal in a Lorentzian is properly given by its area, so that one should be suspicious of a claim that the signal to noise is dramatically increased. That is, the frequency components which give rise to signal and noise cannot be separated by Fourier transforms. Signal to noise can only be increased when it is possible to reject some of the frequency components of the data on the grounds that they contain more noise than signal. This is exactly the criterion which we have used in choosing the truncation point.

There is another property of the discrete Fourier transform which we cannot afford to ignore. A person writing a computer program to perform the deconvolution process will likely use the version of fast Fourier transform available locally[13]). As previously mentioned this algorithm is the discrete version of the Fourier series expansion. The importance of this fact is that the input function is assumed to be periodic and that the original and Fourier space are cyclic; that is, they repeat every 2π. The cyclic nature of Fourier space can have detrimental effects on a deconvolution process when there are lines near the extremes of the original space domain because deconvolution on a cyclic space has the same effect on the element at $2\pi + t$ as it has on an element at t. As a result, the deconvolved spectrum can show the image of a line close to one end of the spectrum at the other end. Since the value of $T(\upsilon)$ at either extreme is theoretically near unity, the array containing $T(\upsilon)$ can simply be augmented by ones until enough space is provided to "protect" one end of the $T(\upsilon)$ array from the other. It is even better to augment the $T(\upsilon)$ array with the function defined by the output of the quadratic least-squares fit to $T(\upsilon)$, i.e., by eq. (12).

Even though the method we use has been described in some detail, one would find it difficult to put it into operation without a knowledge of some of the more subtle nuances of fast Fourier transforms. We refer the reader to the literature[9]) for a detailed explanation of these subtleties; however, we shall list those most pertinent to the present discussion.

The kernel of the fast Fourier transform is complex, as can be seen in eq. (20). For this reason most versions of the fast Fourier algorithm use complex input and output arrays. The $T(\upsilon)$ vector from Mössbauer data is real, however, and one is seemingly forced to double the arithmetic in the transform process merely to accommodate the form of the algorithm. This is not necessary because there are efficient algorithms for transforming real arrays of even length[12]).

To take account of the cyclic nature of the fast Fourier transform, it is necessary to construct the source lineshape vector with symmetry about its first element and its $\frac{1}{2}N+1$ element where N is the dimension of the array.

The last property of fast Fourier transforms to

be treated is one with many mathematical implications. The discrete Fourier transform is defined on a uniform mesh. Thus the velocity array must be redefined from the array provided by the Moiré fringe data such that the velocity increment is constant across the entire velocity range. Since the velocity drive operates in the constant acceleration mode, the velocity increment is nearly constant before any redefinition of the velocity array begins. We have found, however, that some sort of interpolation is necessary to accurately reproduce the data on a uniform mesh. The interpolation procedure is further complicated by a numerical requirement of the discrete Fourier transform.

The discrete Fourier transform is essentially the trapezoidal rule applied to the integral in a Fourier series expansion[9]). For the narrow lines in a Mössbauer spectrum these integrals become less precise as the velocity mesh approaches the linewidth; e.g., in the spectrum of iron metal. We have found that by increasing the number of points in the spectrum before the Fourier deconvolution, we can maintain a much higher accuracy through the deconvolution process.

The interpolation process is to fit the primary $T(\upsilon)$ element, three adjacent points at a time, to a quadratic equation in υ. Within the velocity interval defined by the first two points, we evaluate T by solving the quadratic at the values of υ defined by the new mesh, which fall within the interval. We continue the process by moving the interpolation interval across the entire velocity array, one point at a time, until a new $T(\upsilon)$ array is defined which has a uniform velocity increment and more points than the original array.

We realize that there can be several objections to this treatment, the most powerful of which is that we have created information which we have not measured. This argument would be valid if we tried to present the information as output; however, after the convolution process is complete we restore the data to a uniform velocity mesh which has the same number of points as the original $T(\upsilon)$ array. This final restoration is accomplished by a linear least-squares fit through the points adjacent to each final velocity element. This restoration process is much simpler than it might seem because the final velocity mesh always coincides with the treated array at regular intervals since the number of interpolation points is integral. We note in passing that choosing the number of interpolation points is a complicated matter which must take into account three different properties of the transform: (1) the accuracy of the discrete Fourier transform, (2) the fact that augmentation of the $T(\upsilon)$ must protect it from "end effects", and (3) the fact that the speed and accuracy properties of the discrete transform are maximized when the total number of points in the transformed array is a power of two.

Our reason for choosing a quadratic fit for the formation of the interpolated $T(\upsilon)$ array is that it provides an accurate fit to the data which also conforms to the lineshape present in a Mössbauer spectrum. For example, linear interpolation does not faithfully reproduce sharp peaks in the spectrum. Cubic spline interpolation[14]) has properties which are inconsistent with those of a Lorentzian lineshape. The linear least-squares procedure in the mesh restoration process is sufficient for similar reasons. Furthermore, it takes place after the truncation in Fourier space has removed most of the high-order components of the spectrum which would make a higher-order fit advantageous. The cost of this treatment is additional computer time and slight modifications to the above equations; however, the data is now in a form compatible with the fast Fourier transform process.

There has been much use of the term Debye temperature, θ_D, in the preceding text. Some qualification of the implication of this term is necessary. The Debye temperature is seen by us as an empirically derived parameter to describe easily the dependences of isomer shifts and recoil-free fraction on temperature. Although we report the Debye temperature of our samples and source, we do not mean to imply that this value necessarily implies the highest frequency vibrational mode[15]) in the material. Obviously, a detailed study of vibrational spectra in materials with known Mössbauer Debye temperatures is necessary to demonstrate the theoretical applicability of the Debye model to protein samples. Until this study is completed, the Debye temperature measured by Mössbauer spectroscopists remains a parameter of unknown meaning.

In order to measure the Debye temperature of the source, we take spectra on the same sample but vary the source temperature. By comparing the output of an algorithm based on eq. (3) to the data we obtain a Debye temperature from the second-order Doppler shift. We obtain a Debye temperature based on recoil-free fraction by comparing the same data to

$$f(T) = \exp\left[\frac{-6E_R}{k\theta_D}\left\{\frac{1}{4}+\frac{1}{R^2}\times\right.\right.$$
$$\left.\left.\times\left[\frac{\pi^2}{6}-\sum_{n=1}^{10}\frac{\exp(-nR)}{n^2}(1+nR)\right]\right\}\right], \quad (30)$$

where $f(T)$ is the Debye–Waller factor, E_R is the nuclear recoil energy, and R is θ_D/T.

While we realize that the temperature dependence of isomer shift need not stem only from population differences in the vibrational spectra, we have not as yet found the isomer shift θ_D to differ significantly from the recoil-free fraction θ_D. Nevertheless the possibility always exists that a low lying electronic state can cause a temperature dependence in the isomer shift which will not conform to the Debye model. By measuring θ_D in these two ways and comparing them one has simultaneously a way to check the applicability of the Debye model and a method of finding a low lying excited state which is surely markedly different from the ground state electronically.

The source shape function is determined empirically in a manner analogous to that for θ_D. The source and sample temperatures are held constant while the amount of sample is varied through a set of runs. We vary the source width by trial and error until the output of the Mössbauer data program scales linearly with previous measurements for the amount of sample in each run. We use precision rolled iron foils for this calibration.

In the previous discussion, we have used a Lorentzian line shape for the source function. Although this is the correct line shape for a source displaying the "Heisenberg" width, real sources have greater widths. Therefore, the Lorentzian lineshape becomes doubtful as a correct lineshape function. Reasoning that the "Heisenberg" width Lorentzian is the correct function when one is far from the center of the line, we have chosen two or three Lorentzians of "Heisenberg" widths separated by a variable distance as the source lineshape function. For two lines, the Fourier transform is only slightly more complicated than a simple Lorentzian:

$$S(t) = \exp(-|2\pi\Gamma_s t/N|)\cos(2\pi wt/N), \quad (31)$$

where Γ_s is the halfwidth at half maximum of a "Heisenberg" width Lorentzian (i.e. 0.0476 mm/s for Fe), w is one half the distance between the two Lorentzians in the same units as Γ_s. Here we note that although the cosine function contains zeros which could cause singularities in the deconvolved function in Fourier space, this does not happen because the Fourier space is always truncated within the first point of singularity.

5. Results

5.1. Non-Mössbauer cross-section for iron foil

We measure the absorption coefficient (μ) at 14 keV for iron to be $(498\pm7)\,\text{cm}^{-1}$. This number is the result of a least-squares fit to the plot of detected intensity vs. iron foil thickness with the source velocity at zero. The detected intensity is corrected for background, Compton processes from the 136 and 122 keV radiation, Mössbauer effect resonance and age of the source.

5.2. Debye temperature of the source

The source is 35 mCi of ^{57}Co diffused into 6 μm of rhodium (3 mm diameter). In choosing this source configuration, we are compromising source intensity with self-attenuation in the source and the tendency of the rhodium sources to split magnetically as the source temperature approaches zero. The source Debye temperature is (361 ± 20)K.

The value for the Debye temperature is the weighted average from three different measuring methods for the Debye temperature. The first method is to fit the plot of the output of the quadratic least-squares fit to the transmission array vs source temperature. In the second method, the amount of iron (an output parameter of the data reduction program) is compared to the source temperature. Note that both of the first two methods employ the temperature dependence of the Debye–Waller factor to determine the Debye temperature. In the third method, the isomer shift of the iron metal spectrum is compared to the source temperature. The temperature dependence of the second order relativistic Doppler shift determines the Debye temperature. The value of the Debye temperature from all three determinations agreed within error. Although the Doppler shift measurement was the most precise, it is also the least accurate, potentially, since isomer shift alone can also be a function of temperature due to low lying excited states.

5.3. Source lineshape and resonant cross section

The source lineshape chosen by us was one Lorentzian (fwhm = 0.095) flanked on each side by a Lorentzian (fwhm = 0.095). The two outer Lorent-

zians are centered on the inner Lorentzian, and each had one half the intensity of the inner line. The splitting between centers of the outer lines was 0.055 mm/s. The complex lineshape was determined by two methods.

The first method was to compare the spectra from a 0.001 inch thick stainless steel foil as a function of source temperature. Since this foil has such a strong resonance the data reduction program is stringently tested with respect to its ability to generate a precise lineshape. In addition, the absorption spectrum of stainless steel is such that it is extremely sensitive to the source lineshape. We note here that the variance in the transmission array is highest at the resonance peak of a strong absorber such as stainless steel. For this reason the spectrum of 0.001″ stainless steel is not suitable to the fitting procedures described below. We note here that our choice of source lineshape is based on a trial and error procedure aimed at finding a lineshape of the minimum complexity sufficient to fit the stainless steel data. When a two-line source lineshape failed to provide this complexity, the three-line source shape described above was the least complicated shape to try next. When this shape succeeded, no further shapes were tried.

In the second set of measurements, both the source lineshape and the Mössbauer cross-section are determined. In this set of measurements, the total amount of iron as determined by the Mössbauer program is compared to the thickness of iron foils. The splitting between the centers of the two outer source lines is the only free parameter at this point. If one plots the total iron from the program vs. sample thickness a straight line should result. The source splitting is varied until the straightest line is obtained. From the slope of this line one can determine the Mössbauer cross-section. Our measurement yielded $(2.4 \pm 2) \times 10^{-18}$ cm^2 from the data in fig. 4.

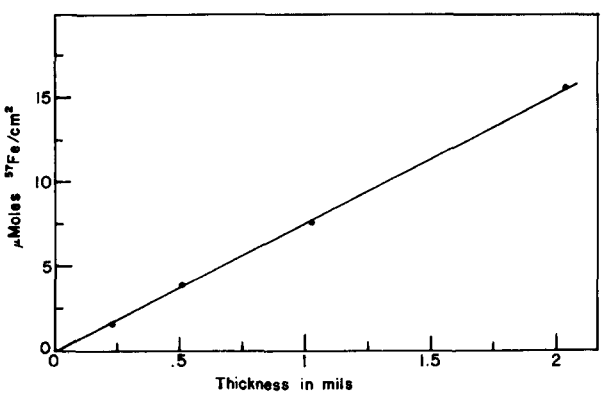

Fig. 4. Total absorption vs thickness of natural iron foils.

5.4. The Debye temperature of iron (NBS# 1541)

The Debye temperature determination for NBS# 1541 yielded (430 ± 30)K and is the weighted average of two different measurements: (1) the Debye temperature measured by the temperature dependence of the isomer shift [(390 ± 30)K], and (2) the Debye temperature measured by the temperature dependence of the Debye–Waller factor [(450 ± 40)K]. Both measurements were made in a similar fashion to that for the source Debye temperature except that the absorber temperature was varied in these runs.

5.5. Mössbauer parameters for iron metal

All the results of these measurements agree with those reported by the group at the Lawrence Livermore Laboratory[16]). Our main purpose here is to demonstrate the precision and accuracy of the spectrometer and data treatment procedures. However, the secondary purpose of this section is to demonstrate by example a statistically valid method of data reduction. Parameters from Mössbauer spectra are used principally to imply atomic properties which in turn imply chemical properties. Because these parameters are twice removed from the chemistry, the Mössbauer spectroscopist must be careful to show the necessity of his fit and to quote the precision of his parameters. We believe that the fitting procedure shown below and the statistic defined in the appendix are equal in importance to the primary data itself. For this reason we show in detail the fitting procedure employed to derive the iron foil parameters.

In order to derive the Mössbauer parameters of any material, one needs the Mössbauer data, a model for the spectrum, a fitting procedure, and a goodness-of-fit criterion. The process of obtaining Mössbauer data is shown above. The goodness-of-fit criterion, ψ^2, is a weighted χ^2 and is described in the appendix. We show the fitting model and fitting procedure below.

Because the largest term, by far, in the iron metal Mössbauer Hamiltonian is the nuclear Zeeman, we can use first-order perturbation theory. Numbering the six lines of iron from left to right we have the following expressions for the line positions:

$$E(1) = \tfrac{1}{2}QS - K(1+R)\,H + D,$$
$$E(2) = -\tfrac{1}{2}QS - K(1+\tfrac{1}{3}R)\,H + D,$$
$$E(3) = -\tfrac{1}{2}QS + K(\tfrac{1}{3}R-1)\,H + D,$$
$$E(4) = -\tfrac{1}{2}QS - K(\tfrac{1}{3}R-1)\,H + D,$$
$$E(5) = -\tfrac{1}{2}QS + K(1+\tfrac{1}{3}R)\,H + D,$$
$$E(6) = \tfrac{1}{2}QS + K(1+R)\,H + D,$$

where QS is the span of the diagonal components of the nuclear quadrupole matrix when the magnetic hyperfine matrix is diagonal. Therefore, only a range for the components of the electric field gradient tensor is implied by QS. K equals 5.9175 mm/s and uses the published value for the magnetic moment of the ground state of ^{57}Fe, +0.09024 nm[17]). R is the magnetic moment ratio of the excited to ground state of ^{57}Fe. H is the value of the internal field of ^{57}Fe in MG. D is the isomer shift.

The line intensities are:

$$I(1) = C,$$
$$I(2) = \tfrac{2}{3}BC,$$
$$I(3) = \tfrac{1}{3}C,$$
$$I(4) = \tfrac{1}{3}C,$$
$$I(5) = \tfrac{2}{3}BC,$$
$$I(6) = C,$$

where C is the peak height of the spectrum, B is a fudge factor for lines 2 and 5, related to the average magnetic polarization angle of the foil[18]).

The remaining parameters for the fit to the data are the linewidth to be used with the shape function in eqn. (15) and the value for the baseline. Both the linewidth and B are fixed during any run of the fitting program. There are thus six free parameters in the fit: QS, R, H, D, C, and the baseline. The baseline is eliminated as a free parameter by requiring that the sum of trial vector elements equal the sum of the experimental vector elements.

The fitting procedure consists of minimizing the value of ψ^2 by varying the values of QS, R, H, D and C from an initial guess at their values. Convergence of the minimization algorithm is a difficult problem in general; however, we have found that the following system converges to a true minimum; i.e., a minimum which cannot be improved by the parabolic approximation scheme described below. The parameters QS, D and C are minimized by finding the ψ^2 corresponding to three values of a parameter around its current value. The three points define a parabola which is solved for a minimum which becomes the next value for the parameter. The two parameters R and H are coupled so that varying one without the other can lead to a false minimum. Therefore each of the five parameters is minimized in turn until an overall minimum is found. R and H are minimized together every third turn.

There are other components to the minimization program which speed convergence; however, their discussion is unnecessary since they do not affect the final values of the parameters. The essential point here is that not only is ψ^2 minimized but that it is minimized in such a way that one can easily obtain the uncertainties in the parameters. Thus the parameters C, QS and D can be varied from their minimum values individually until ψ^2 becomes greater than its 95% confidence contour. The value of these parameters at this contour defines the 95% confidence interval for the parameter. R and H must be varied together along their minimum slope angle in the R–H plane, where ψ^2 is viewed as a function of R and H only. However, this angle is easily calculable in this case, so that we can obtain the 95% confidence range easily for R and H. We contrast this to the situation occurring if the six lines were fit individually. Here the 95% confidence contour is along the minimum slope angle in the R, H, QS, D and H 5-plane where ψ^2 is viewed as a function of all five parameters. We note that the confidence ranges of the parameters must be greater than those from our model because the uncertainty in any parameter will contain cross terms with the other parameters in addition to the terms from our model.

Our last pitfall for the curve fitter is the goodness-of-fit criterion. The weakness of the χ^2 criterion is that all the points are assumed to have equal variance and equal information. Although the points in a Mössbauer spectrum have approximately equal variance, the points at the extremes of a spectrum contain no information on the Mössbauer parameters. For these reasons, the χ^2 distribution is not appropriate as a basis for confidence-interval tests for Mössbauer parameters. The quantity, ψ^2, which we define in the appendix, has none of these weaknesses.

The results of our curve fitting procedure on three iron foil (NBS#1541) runs at different temperatures are summarized in table 2. Our laboratory is principally biophysics oriented, so we chose not to attempt a microscopic physical interpretation of the iron foil data. In addition, all these

TABLE 2
Fitting parameters for iron (NBS #1541).

Temp (K)	4.2	101	291
C	1.44±0.04	1.39±0.04	1.33±0.04
H (kG)	339.2±0.4	338.2±0.4	330.4±0.4
R	1.715±0.005	1.715±0.005	1.715±0.005
δ(mm/s)	−0.002±0.005	0.000±0.005	0.002±0.005
QS (mm/s)	0.002±0.007	0.006±0.007	0.005±0.007
s	0.0239	0.0199	0.0221
B	1.32	1.32	1.32
fwhm	0.165	0.165	0.165
minimum ψ^2	4.81	5.55	3.93
counts/ channel	57 000	57 000	57 000

data are consistent with the previously reported values. However, the interesting quality of these data is that they were obtained from three Mössbauer runs: each with 57 000 counts per channel. We expect this degree of precision and accuracy to aid considerably in our attempts to use Mössbauer spectroscopy in our studies of multi-iron proteins. In the preceding, we have shown the methods and results of many measurements from this spectrometer. We emphasize that it is the methods rather than the results which are important here. The compatibility of the results with the previous measurements merely validates the accuracy and precision of the spectrometer. The innovative aspects of this spectrometer are that it provides a known absorber lineshape, that it is quantitative, and that it provides information on the vibrational states of the absorber.

In order to add emphasis to the innovative aspects of the above approach to Mössbauer spectroscopy we have included fig. 5. This figure shows the absorption spectra, inverted and normalized to the transmission spectra of the oxidized spinach ferredoxin sample mentioned in the introduction. Two points are of chief interest here. The first is the depth of the resonances of the transmission spectra. The previously published spectra, including our own, have greatly underestimated the depth of the resonances for quadrupole pairs at low applied magnetic field. For example, the leftmost line in part (a) has a percent transmission minimum of 60% which corresponds to an absorption maximum of 1.2 o.d. (shown as a solid line). The second point is the obvious increase in resolution of the absorption spectra compared to the transmission spectra. In part (a) of the figure, the

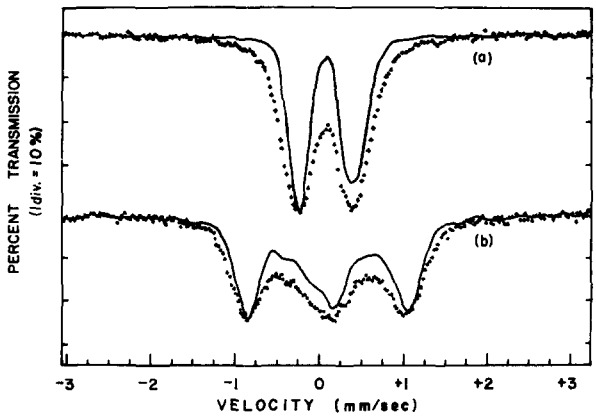

Fig. 5. Transmission spectra (crosses) superimposed by absorption spectra (solid lines) for oxidized spinach ferredoxin at 4.2 K: (a) $H = 1.15$ kG, (b) $H = 46$ kG.

absorption spectra show an inequivalence in the two lines not at all obvious in the transmission spectra.

Appendix

By applying Poisson statistics to eqs. (10) and (29) we derive the variance in the deconvolved data:

$$s^2 = \frac{N_T}{f_s^2 N_0^2}\left(\frac{\exp(4\pi\Gamma_s T/N) - 1}{2\pi\Gamma_s}\right), \tag{32}$$

where N_T is the number of counts per channel off resonance and N_0 is the number of counts per channel of 14 keV gammas.

We define ψ^2 as follows:

$$\psi^2 = \sum_{i=1}^{n} \frac{(x_i - \theta_i)^2\, a_i}{s^2}, \tag{33}$$

where x_i and θ_i are the experimental and expected data respectively for an absorption spectrum, and

$$a_i = |\theta_i| \Big/ \sum_{i=1}^{n} |\theta_i| . \tag{34}$$

We note that this function is simply a weighted χ^2. In the following section, we derive the variance and expectation value for the ψ^2 distribution.

Let

$$\xi_i = \frac{x_i - \theta_i}{s},$$

then ξ is a random variable with an expectation value of zero and a variance of one. (Here we recall that one of the restraints in the fitting program is that the sum of the x_i equals the sum of

the θ_i.) If $\eta = \xi^2 a$, then η is a random variable with an expectation value, a, and a variance, $2a^2$ [see p. 233 Cramér[12])]. Therefore, the variable

$$\psi^2 = \sum_{i=1}^{n} \eta_i \tag{35}$$

has expectation [see p. 191 Cramer[12])]

$$m = \sum_{i=1}^{n} a_i = 1, \tag{36}$$

and variance

$$\sigma^2 = \sum_{i=1}^{n} 2a_i^2. \tag{37}$$

Theoretically, the frequency function for ψ^2 need not be normal, i.e., Gaussian. However, we performed the required convolution numerically for an iron spectrum and found that the resulting function was very nearly Gaussian with the theoretical mean and variance. The iron spectrum represents a "worst case" situation since the six sharp lines in this spectrum tend to reduce the sums in eqs. (36) and (37) to their smallest number of terms. As the resonance appears broader the ψ^2 distribution approaches the χ^2 distribution, which itself is normal when the number of terms is greater than 30.

If the distribution of ψ^2 is normal, then the 95% confidence contour is at $1+1.96\sigma$. We note here that even if the distribution is not normal the value for the 95% contour will not be greatly affected since σ is a theoretically correct number and the contour is near 2σ above the mean value.

This work was supported by United States Public Health Service grant #GM12176. We are also grateful to the following for their consistently valuable advice: K. Efferson and D. Coffey from American Magnetics. Inc., J. Spikermann from Ranger Engineering Corp., and L. Jensen and R. Kushler from the University of Michigan Statistics Department.

References

1) W. R. Dunham, G. Palmer, R. H. Sands, A. J. Bearden and W. H. Orme-Johnson, Biochem. Biophys. Acta **253** (1971) 134.
2) R. M. Polichar, W. R. Dunham and R. H. Sands, in preparation.
3) American Magnetics, Inc., 461 Laboratry Rd., Oak Ridge, Tenn. 37830, U.S.A.
4) Cryogenic Associates, 1718 N. Luett Ave., Indianapolis, Ind. 46222, U.S.A.
5) Ranger Engineering Corp., 3132 Bryan St., Fort Worth, Texas 76110, U.S.A.
6) Northern Scientific, Inc., 2551 W. Beltline, Middleton, Wis. 53562, U.S.A.
7) Chu Tzu Wu, Thesis (University Microfilms, Ann Arbor Mich.) order °76-9549.
8) Ortec, Inc., 100 Midland Rd., Oak Ridge, Tenn. 37830, U.S.A.
9) E. O. Brigham, *The fast fourier transform* (Prentice Hall, Englewood Cliffs, N.J., 1974).
10) M. D. C. Ure and P. A. Flinn, Mössbauer effect meth. 7 (1971) 245.
11) F. Oberhettinger, *Fourier transforms of distributions and their inverses* (Academic Press, New York 1973).
12) Cramer, H., *Mathematical methods of statistics* (Princeton University Press, N.J., 1946).
13) L. J. Harding, The discrete fourier transform, Computer Center Memo 327, University of Michigan Computer Center, Ann Arbor, Mich. (1975).
14) J. H. Ahlberg, E. N. Nilson and J. L. Walsh, *The theory of splines and their applications* (Academic Press, New York, 1967).
15) J. E. Mayer, and M. G. Mayer, *Statistical mechanics* (J. Wiley, New York, 1963).
16) C. E. Violet, and D. N. Pipkorn, J. Appl. Phys. **42** (1971) 4339.
17) R. P. Lochner, and S. Geschwind, phys. Rev. **139** (1965) A991.
18) R. S. Preston, S. S. Hanna and J. Heberle, phys. Rev. **128** (1962) 2207.